

anti-CD11b, anti-CD4, anti-CD8 α , and anti-CD45R/B220. Binding of primary antibodies was detected as described (16). Percentages of infiltrating cells were calculated from a minimum of 1000 infiltrating cells counted on representative heart sections.

18. Supplemental web material for Fig. 2 (analysis of splenic cell populations) is available at www.sciencemag.org/feature/data/984504.shl.

19. Splenocytes were harvested 21 days after the initial immunization with FCA, ChTR1, or M7A α , and subpopulations were analyzed by fluorescence-activated cell sorting. Specific antibodies to rat IgG (all purchased from Pharmingen) were as follows: anti-CD11b, anti-CD4, anti-CD8 α , and anti-CD45R/B220.

20. Spleens from M7A α -, ChTR1-, or k κ -immunized BALB/c mice (10) were removed 21 days after the first immunization, and T cells were enriched by negatively sorting out CD11b-, Gr1-, and B220-expressing cells with specific antibodies conjugated to magnetic beads (Dyna, Oslo, Norway). In 96-well plates, T cells (1×10^5 T cells per well) were cultured with γ -irradiated syngeneic splenocytes (5×10^5 cells per well) pulsed with M7A α , ChTR1, or k κ peptide (each at 50 μ g/ml). To measure proliferation, we harvested cultures 3 days later after overnight addition of 1 μ Ci of [3 H] thymidine. It should be noted that 10 days after the initial immunization, T cell reactivity is already observed, that is, at a time when no histopathological signs of myocarditis are present.

21. For adoptive transfer of ChTR1 peptide-induced inflammatory heart disease into nonimmunized recipient mice, 6-week-old donor BALB/c mice were immunized twice with ChTR1 peptide in FCA or with FCA only (10). Twenty-one days after the initial immunization, splenic T cells (20) were cultured with γ -irradiated syngeneic splenocytes pulsed with ChTR1 peptide (50 μ g/ml) for 4 days in the presence of mrlL-2 (50 U/ml). Recipient BALB/c mice were injected intraperitoneally with lipopolysaccharide (25 μ g per mouse) on days 0 and 4, and 1×10^6 in vitro-stimulated cells from immunized donor mice were injected intravenously on day 7 (7). Transferred donor T cells (>95%) had a TCR $\alpha\beta^+$ CD4 $^+$ CD69 $^+$ CD25 $^+$ phenotype.

22. K. Bachmaier *et al.*, *J. Immunol.* **157**, 1752 (1996).

23. Twenty-one days after the initial immunization (10), serum was collected and specific antibody production was determined by enzyme-linked immunosorbent assay (ELISA) (6). Briefly, 96-well plates were coated with 2 μ g of peptide per well. Diluted mouse sera (1:100) were allowed to bind to the plates, washed, and binding was detected with horseradish peroxidase-conjugated antibody to mouse IgG (Sigma, #A-3673). Substrate (ABTS, Sigma, #A-1888) conversion was detected measuring absorbance at 405 nm.

24. A. M. Krieg *et al.*, *Nature* **374**, 546 (1995); H. L. Davis *et al.*, *J. Immunol.* **160**, 870 (1998); J. P. Messina, G. S. Gilkeson, D. S. Pisetsky, *ibid.* **147**, 1759 (1991).

25. CpG motive-containing synthetic oligodeoxynucleotides (ODNs) were derived either from *C. trachomatis* DNA (CpG 1) or from previously reported bacterial DNA sequences (CpGs 2 and 3) (24). ODNs were phosphorothioate modified to increase their in vivo stability. ODNs (30 μ g in 100 μ l of 0.15 mM NaCl buffer) were administered ip at the time of the immunizations. BALB/c mice were subcutaneously immunized twice at a 7-day interval with the M7A α peptide (50 μ g per mouse) in a 1:1 emulsion with mineral oil [Freund's incomplete adjuvant (FIA)] (8, 10). Twenty-one days after the initial immunization hearts were analyzed for the presence and severity of myocarditis.

26. M. Maass, C. Bartels, P. M. Engel, U. Mamat, H. H. Sievers, *J. Am. Coll. Cardiol.* **31**, 827 (1998); M. Maass, E. Krause, P. M. Engel, S. Kruger, *Angiology* **48**, 699 (1997); L. A. Jackson *et al.*, *Am. J. Pathol.* **150**, 1785 (1997); C. C. Kuo *et al.*, *Proc. Natl. Acad. Sci. U.S.A.* **92**, 6911 (1995); C. A. Gaydos, J. T. Summersgill, N. N. Sahney, J. A. Ramirez, T. C. Quinn, *Infect. Immun.* **64**, 1614 (1996); C. C. Kuo *et al.*, *J. Infect. Dis.* **167**, 841 (1993).

27. T. C. Moazed, C. Kuo, J. T. Grayston, L. A. Campbell, *J. Infect. Dis.* **175**, 883 (1997); J. B. Muhlestein *et al.*, *Circulation* **97**, 633 (1998); I. W. Fong *et al.*, *J. Clin.*

Microbiol. **35**, 48 (1997); T. C. Moazed, C. Kuo, D. L. Patton, J. T. Grayston, L. A. Campbell, *Am. J. Pathol.* **148**, 667 (1996).

28. M. Odeh, A. Oliven, S. Rauchfleisch, H. Bassan, *J. Intern. Med.* **229**, 289 (1991); J. T. Grayston, C. H. Mordhorst, S. P. Wang, *J. Am. Med. Assoc.* **246**, 2823 (1981); C. Y. Tong, F. Potter, E. Worthington, P. Mullins, *Lancet* **346**, 710 (1995); L. Wesslen *et al.*, *ibid.* **340**, 427 (1992); F. Diaz and J. Collazos, *Scand. J. Infect. Dis.* **29**, 93 (1997).

29. Supplemental web material for Fig. 3 (arterial wall thickness ratios) is available at www.sciencemag.org/feature/data/984504.shl.

30. For the morphometrical analysis of arteries, inner and outer diameters of individual arteries were measured and the ratio between wall thickness (outer diameter minus inner diameter) and outer diameter was calculated [T. Matsusaka *et al.*, *J. Clin. Invest.* **98**, 1867 (1996)]. At least five arteries with a minimum inner diameter of 50 μ m were analyzed per individual heart.

31. The *C. trachomatis* mouse pneumonitis (MoPn) biovar (strain Nigg II) was purchased from the American Type Culture Collection (Rockville, MD) and grown in HeLa-229 cells. Elementary bodies were purified, stored, titered, and prepared for infection as described [S. Pal, I. Theodor, E. M. Peterson, L. M. de la Maza, *Infect. Immun.* **65**, 3361 (1997)]. Eight-week-

old female BALB/c mice were inoculated either intranasally with 0 (sham), 1×10^3 , 1×10^4 , 1×10^5 , or 1×10^6 *C. trachomatis* MoPn inclusion-forming units (IFUs), or intravaginally with 0 (sham), 1×10^4 , 1×10^5 , 1×10^6 , or 1×10^7 IFU of *C. trachomatis* MoPn.

32. T. C. Quinn *et al.*, *J. Am. Med. Assoc.* **276**, 1737 (1996).

33. Z.-S. Zhao, F. Granucci, L. Yeh, P. A. Schaffer, H. Cantor, *Science* **279**, 1344 (1998); N. K. Maclaren and M. A. Alkinson, *Mol. Med. Today* **3**, 76 (1997); J. F. Bach, *Endocr. Rev.* **15**, 516 (1994); M. G. von Herrath and M. B. Oldstone, *Curr. Opin. Immunol.* **8**, 878 (1996); P. S. Ohashi, *ibid.*, p. 808.

34. J. B. Zabriske and J. E. Friedman, *Adv. Exp. Med. Biol.* **161**, 457 (1983); M. B. Oldstone, *Cell* **50**, 819 (1987); C. A. Janeway, *Immunity* **8**, 391 (1998); M. S. Horwitz *et al.*, *Nature Med.* **4**, 781 (1998).

35. We thank M. Saunders for critical reading of the manuscript; P. S. Ohashi, T. W. Mak, Y. Y. Kong, A. Oliveiros-Santos, Q. Liu, C. Pummerer, T. Sasaki, P. Liu, and I. Kozieradzki for helpful comments; and the Amgen Protein Synthesis group and C. Richardson for providing peptides and advice. K.B. is a Fellow of the Heart and Stroke Foundation of Canada. J.M.P. is supported by the Medical Research Council of Canada.

13 November 1998; accepted 20 January 1999

Prion Domain Initiation of Amyloid Formation in Vitro from Native Ure2p

Kimberly L. Taylor,¹ Naiqian Cheng,² Robert W. Williams,³ Alasdair C. Steven,² Reed B. Wickner^{1*}

The [URE3] non-Mendelian genetic element of *Saccharomyces cerevisiae* is an infectious protein (prion) form of Ure2p, a regulator of nitrogen catabolism. Here, synthetic Ure2p¹⁻⁶⁵ were shown to polymerize to form filaments 40 to 45 angstroms in diameter with more than 60 percent β sheet. Ure2p¹⁻⁶⁵ specifically induced full-length native Ure2p to copolymerize under conditions where native Ure2p alone did not polymerize. Like Ure2p in extracts of [URE3] strains, these 180- to 220-angstrom-diameter filaments were protease resistant. The Ure2p¹⁻⁶⁵-Ure2p cofilaments could seed polymerization of native Ure2p to form thicker, less regular filaments. All filaments stained with Congo Red to produce the green birefringence typical of amyloid. This self-propagating amyloid formation can explain the properties of [URE3].

Genetic evidence identified [URE3] and [PSI], two nonchromosomal genes of *Saccharomyces cerevisiae*, as prions of Ure2p and Sup35p, respectively, which implies that proteins can be hereditary material (1). In response to a good nitrogen source (ammonia or glutamine), Ure2p blocks assimilation of poor nitrogen sources by blocking the action

of the transcription regulator Gln3p (2). Sup35p is a subunit of the translation release factor (3). [URE3] (4) and [PSI] (5) are altered forms of Ure2p and Sup35p that have lost their normal functions but have acquired the ability to convert their normal forms into the altered (prion) form (1), a notion supported by genetic and biochemical data (6-10). The prion concept originates in studies of the spongiform encephalopathies (11), believed due to a self-propagating altered form of PrP that forms scrapie-associated filaments and amyloid deposits in brains of affected animals (12).

Amyloid is defined as a filamentous protein structure that stains with the dye Congo Red (CR) to produce green birefringence under polarized light and is characterized by protease resistance and an antiparallel β sheet structure (13). Amyloid deposits of the A β peptide ac-

¹Laboratory of Biochemistry and Genetics, National Institute of Diabetes and Digestive and Kidney Diseases, National Institutes of Health, Bethesda, MD 20892-0830, USA. ²Laboratory of Structural Biology, National Institute of Arthritis and Musculoskeletal and Skin Diseases, National Institutes of Health, Bethesda, MD 20892-2717, USA. ³Department of Biochemistry and Molecular Biology, Uniformed Services University for Health Sciences, Bethesda, MD 20814, USA.

*To whom correspondence should be addressed. E-mail: wickner@helix.nih.gov

REPORTS

accumulate in the brain of patients with Alzheimer's disease, and amyloid deposits of overproduced monoclonal immunoglobulins are found in patients with certain B cell neoplasms.

The 354-residue Ure2p is normally a dimer (14). Overexpression of the first 65 residues of Ure2p (the prion domain) induces de novo formation of the [URE3] prion at >1000-fold the spontaneous rate (6). Deletion of the first 65 residues leaves a COOH-terminal fragment (the nitrogen regulation domain) competent in nitrogen regulation but unaffected by the [URE3] prion (6). The prion domain can also propagate [URE3] in the absence of the nitrogen regulation domain (10). Thus, the NH₂-terminal 65 residues are necessary for Ure2p to be altered to the prion form and sufficient to induce the change in normal Ure2p.

Synthetic Ure2p¹⁻⁶⁵ (15) in 6 M guanidine (16) was diluted 1:40 into buffer. A fine precipitate was first visible at 20 min and was complete after 1 hour, with >90% of the peptide in the precipitate. Negative staining electron microscopy of the precipitate showed thin straight filaments (Fig. 1A), which were variable in width because of lateral bundling of variable numbers of narrow protofilaments. Individual protofilaments are uniformly 40 to 45 Å in diameter.

In an attempt to reproduce in vitro the in vivo induction of the [URE3] prion by Ure2p¹⁻⁶⁵, we diluted denatured synthetic Ure2p¹⁻⁶⁵ into purified native Ure2p (17). Equimolar amounts of Ure2p¹⁻⁶⁵ precipitated about 80% of Ure2p in <4 hours (Fig. 2). When 10- and 100-fold less Ure2p¹⁻⁶⁵ was added, precipitation of Ure2p decreased by 9.4- and 30-fold, respectively, indicating that the aggregate was roughly a 1:1 mixture of protein and peptide. When we added equimolar Ure2p¹⁻⁶⁵ to bovine serum albumin or a mixture of standard proteins (16), none of these proteins entered the peptide precipitate (Fig. 2), which suggests that Ure2p¹⁻⁶⁵ interacts specifically with Ure2p. When we added nonprion domain peptide residues 148 to 213 of Ure2p to Ure2p in equimolar amounts, no precipitate was formed. When we used Aβ peptide, the major component of amyloid in Alzheimer's disease, to generate amyloid filaments in vitro under the same conditions (16, 18), Ure2p was not incorporated into the precipitate (Fig. 2), again showing the specificity of the interaction of Ure2p¹⁻⁶⁵ with native Ure2p.

Electron microscopy of Ure2p¹⁻⁶⁵-Ure2p copolymers (Fig. 1B) revealed filaments 180 to 220 Å wide, much wider than the prion domain filaments (Fig. 1A). The copolymer filaments were not hollow, as judged by the absence of a stain-penetrable lumen. No filaments were observed in soluble Ure2p without Ure2p¹⁻⁶⁵, and Ure2p formed only amorphous aggregates when heated at 100°C for 5 min (19).

Ure2p is protease-resistant in extracts of [URE3] strains compared to isogenic [ure-o] strains (6). We compared protease resistance of filaments of Ure2p¹⁻⁶⁵ and of Ure2p¹⁻⁶⁵-Ure2p with that of native Ure2p and heat-

denatured Ure2p (20) (Fig. 3). Native Ure2p was digested in <2 min, whereas the filaments were digested more slowly. The 7-kD Ure2p¹⁻⁶⁵ persisted for >20 min. In the Ure2p¹⁻⁶⁵-Ure2p sample, fragments of 30 to

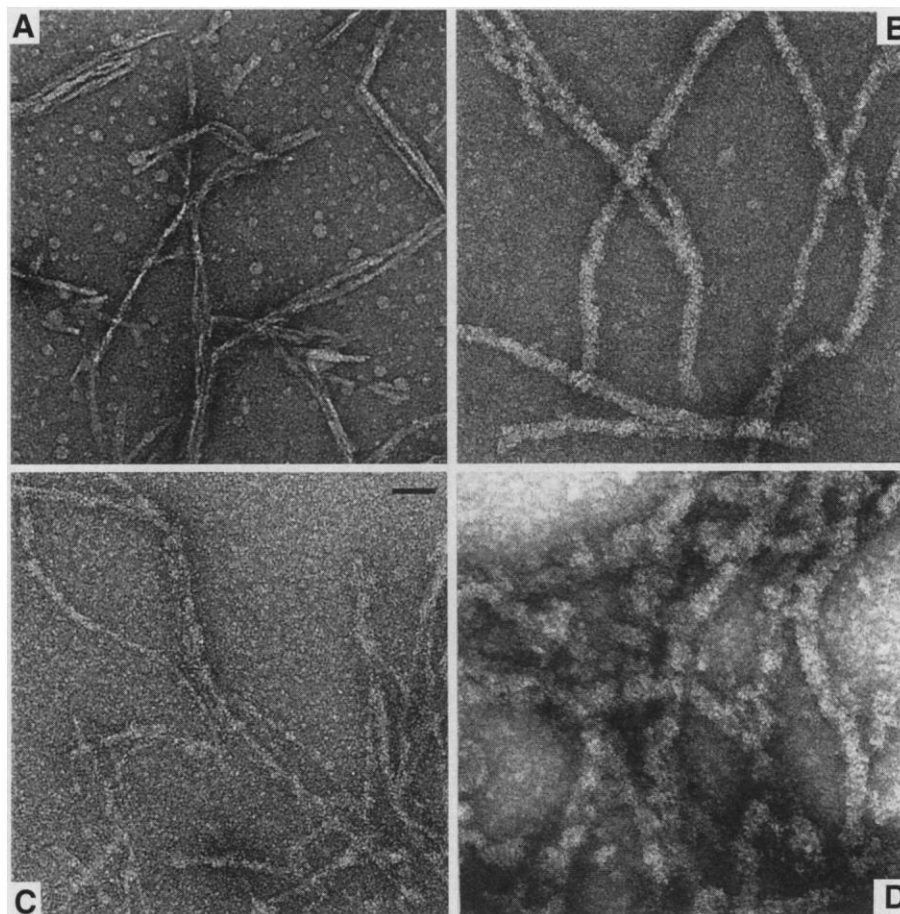


Fig. 1. Electron microscopy of negatively stained filaments formed by polymerization of Ure2p and its prion domain Ure2p¹⁻⁶⁵. (A) Filaments of Ure2p¹⁻⁶⁵, consisting of parallel bundles of 45 Å protofilaments. (B) Cofilaments of Ure2p and Ure2p¹⁻⁶⁵. (C) Cofilaments after digestion with proteinase K (20). Bar = 500 Å. (D) Filaments produced by seeding a solution of 66.4 µg of Ure2p with 1.7 µg of copolymer filaments. Drops of samples at 13 µM protein or peptide [6.5 µM for sample (C)] were applied to freshly glow-discharged carbon-collodion films mounted on electron microscope grids, negatively stained with 1% uranyl acetate, and observed in a Philips CM120 electron microscope. Although the axial regularity of filaments in (A) and (B) implies that they are ordered structures, no axial repeats were detected by Fourier analysis of the images (19). A report of filament formation by the NH₂-terminal domain of Sup35p aged for 1 week at pH 2 (25) also alludes to filament formation by the Ure2p prion domain under these conditions, but these filaments were not described.

Table 1. Secondary structure of Ure2p preparations. Raman spectroscopy, data collection, and analysis have been described (31). Protein solutions were 10 to 30 mg/ml in 50 mM phosphate buffer (pH 8.0) containing 0.2 M NaCl. The Raman amide I and amide III spectra were analyzed for secondary structure information by the nonnegative least-squares approach.

Sample	Raman amide I		Raman amide III	
	α helix	β sheet	α helix	β sheet
Ure2p ¹⁻⁶⁵ filaments	0 ± 4	65 ± 5	8 ± 6	60 ± 5
Ure2p soluble	36 ± 5	30 ± 4	45 ± 5	30 ± 6
Ure2p ¹⁻⁶⁵ -Ure2p filaments	6 ± 5	55 ± 4	25 ± 5	45 ± 6
Ure2p in mixed filaments*	14 ± 5	49 ± 4	32 ± 5	40 ± 6

*Conformation of Ure2p in the mixed (Ure2p¹⁻⁶⁵-Ure2p) filaments was estimated by subtracting 0.16 [= 65/(65 + 354)] times the Ure2p¹⁻⁶⁵ spectrum from that of the Ure2p¹⁻⁶⁵-Ure2p filaments.

REPORTS

32 kD persisted for about 2 min and fragments of 7 to 10 kD—larger than the 7-kD Ure2p¹⁻⁶⁵—persisted for over 20 min. Heat-denatured Ure2p showed lower overall protease resistance and lacked the persistent 7- to 10-kD species. The pattern of protease resistance in the Ure2p¹⁻⁶⁵-Ure2p fiber is similar to that observed in [URE3] extracts (6), indicating that a change, similar to that found in [URE3] strains, occurred when Ure2p was precipitated by Ure2p¹⁻⁶⁵.

Electron microscopic examination of the protease-treated Ure2p¹⁻⁶⁵-Ure2p cofilaments showed filaments of variable width (Fig. 1C) but generally narrower than the starting material. Like the prion domain protofilaments (Fig. 1A), the narrowest segments

were about 45 Å wide, straight, and lacked visible substructure. Thus a copolymer filament apparently had a backbone of a prion domain protofilament surrounded by the remainder of Ure2p. The latter portion was digested by proteinase K, with accumulation of the resistant 7- to 10-kD fragment.

Without the green birefringence, binding CR is not indicative of amyloid structure (21). When stained with CR (22), all Ure2p precipitates appeared red under bright field, indicating that they bound the dye, but under polarized light the heat-denatured Ure2p appeared dark (19), whereas Ure2p¹⁻⁶⁵-Ure2p and Ure2p¹⁻⁶⁵ filaments had an apple-green birefringence (Fig. 4). This showed that they were amyloid fibers, unlike the heat-denatured material,

which, as observed by electron microscopy, was an amorphous precipitate.

Ure2p¹⁻⁶⁵-Ure2p and Ure2p¹⁻⁶⁵ filaments bound 14.8 and 3.0 CR molecules per monomer, with dissociation constant (K_d) values of 1.7 and 0.81 μ M, respectively (23). Dye bound to both precipitates also exhibited a spectral shift with a maximum difference at 540 nm, which is typical of amyloid fibers.

Native Ure2p contains both α helix and β sheet (Table 1). The Ure2p¹⁻⁶⁵ filaments were predominantly β sheet with little or no helix structure. The Ure2p¹⁻⁶⁵-Ure2p copolymer was also high in β sheet. Assuming that Ure2p¹⁻⁶⁵ has the same structure in the copolymer as in the Ure2p¹⁻⁶⁵ filaments, we estimate that Ure2p in the cofilaments has significantly increased β sheet and decreased α helix compared with its native structure (Table 1).

Addition of 3 μ l (1.7 μ g) of Ure2p¹⁻⁶⁵-Ure2p cofilaments to 123 μ l (66.4 μ g) of native Ure2p resulted, after 2 weeks at 4°C, in precipitation of 62% of the native Ure2p. Filaments 290 to 400 Å in diameter (Fig. 1D) that showed green birefringence with CR were observed (Fig. 4). Proteinase K digestion of these filaments produced a pattern of resistant fragments similar to that observed with Ure2p¹⁻⁶⁵-Ure2p cofilaments (Fig. 3). The amounts of resistant fragments observed were far in excess of the small amount of seed filament used, showing that the protease-resistant material was not simply carried over from the seed filaments. Thus the Ure2p amyloid formation is a seeded process capable of continued propagation in vitro.

We suggest that the filament structure formed by Ure2p¹⁻⁶⁵ also forms the core of the equimolar cofilament with intact Ure2p and of the propagated fiber composed mainly of intact Ure2p, with the prion domain stacking in β sheets and the COOH-terminal domain protruding to form the wavy, thicker structure.

Does the amyloid formation demonstrated

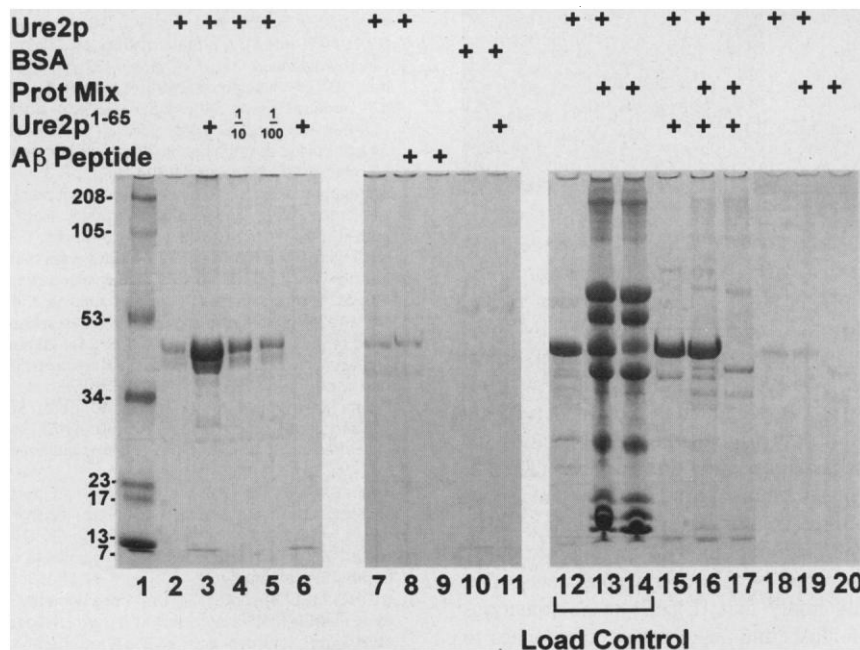
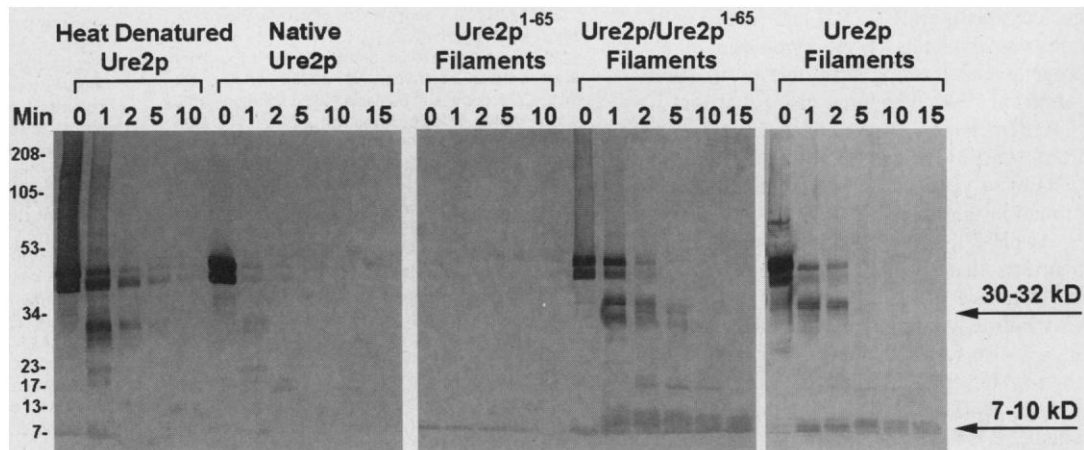


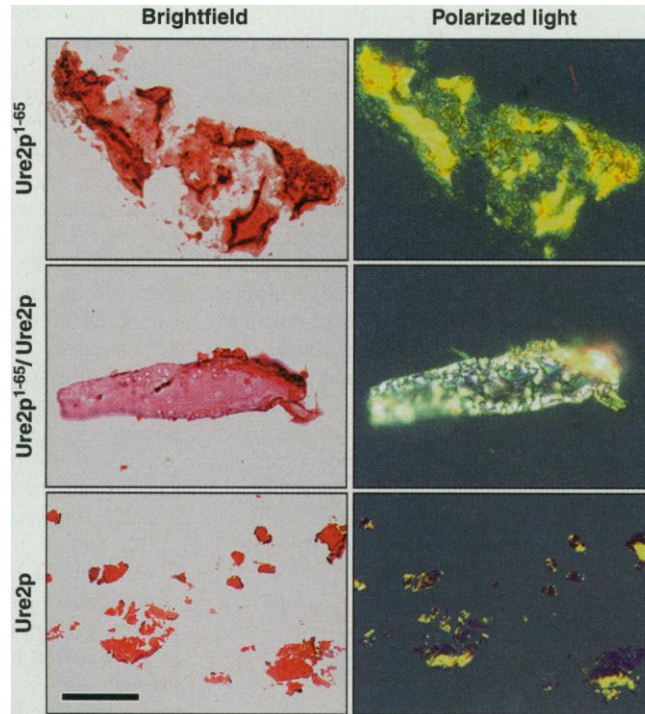
Fig. 2. Filament formation by Ure2p¹⁻⁶⁵ specifically precipitates intact native Ure2p. Native Ure2p alone, or with a mixture of other proteins, was incubated with Ure2p¹⁻⁶⁵ (76). Washed precipitates were analyzed by SDS-PAGE and stained with Coomassie blue. Lanes 12 to 14 show total amounts added to mixtures; other lanes show only the precipitate. BSA, bovine serum albumin.

Fig. 3. Proteinase K resistance of Ure2p incorporated into filaments with Ure2p¹⁻⁶⁵ (20). Heat-denatured Ure2p, untreated native Ure2p, Ure2p¹⁻⁶⁵ filaments, cofilaments formed by an equimolar mixture of Ure2p¹⁻⁶⁵ and native Ure2p, and filaments of Ure2p seeded by cofilaments were treated with proteinase K for various times and the products were analyzed by immunoblotting with a Ure2p antibody specific for the NH₂-terminus. The seeded filaments of Ure2p (last sample) consisted of 1.7 μ g of seed and a further 38 μ g of precipitated full-length Ure2p.



REPORTS

Fig. 4. CR birefringence of Ure2p¹⁻⁶⁵, Ure2p¹⁻⁶⁵-Ure2p, and Ure2p fibers seeded by mixed filaments. Filaments were stained with CR and observed at ×100 magnification under bright field (left) or by polarization microscopy (right) (22). Bar = 20 μm.



here for Ure2p¹⁻⁶⁵ and the Ure2p¹⁻⁶⁵-Ure2p mixture correspond to the [URE3] prion? The in vitro amyloid fibers show a pattern of protease resistance like that observed for Ure2p in extracts of [URE3] strains. Moreover, it is specifically the prion domain (residues 1 to 65) that induces the amyloid formation with intact native Ure2p. Neither Ure2p¹⁴⁸⁻²¹³ (part of the nitrogen regulation domain) nor the Alzheimer's Aβ peptide shows this activity, although the latter does form amyloid. The seeding by cofilaments of amyloid formation by native Ure2p suggests that, as in vivo, the in vitro reaction can propagate. Further, Ure2p-green fluorescent protein fusion proteins have been found to form intracellular aggregates in vivo specifically in [URE3] cells (24). We suggest that, in [URE3] cells, amyloid filaments recruit most of the Ure2p in the cytoplasm. Ure2p in filaments is inactive or unable to enter the nucleus. Mating of [URE3] and [ure-o] cells transmits filaments to the cytoplasm of all progeny cells, which seed further filament formation. However, final proof that this is [URE3] requires characterization of Ure2p from [URE3] strains and transmission of [URE3] to yeast cells by amyloid filaments formed in vitro.

At pH 2 the Sup35p prion domain forms filaments that show birefringence with CR and slightly increased protease resistance (25). Full-length Sup35p, made in *Escherichia coli*, also forms filaments, but these show no green birefringence with CR (26). Sup35p is aggregated in [PSI] strains (8, 27), but whether it is in an amyloid form has not been reported.

In Alzheimer's disease, a peptide fragment of a large precursor protein forms the amyloid. In vitro amyloid formation by the monoclonal light chains produced by some multiple myelomas occurs only after partial proteolysis (28). In parallel with in vivo results (6, 10), we found that native Ure2p did not form amyloid filaments (29) unless the prion domain peptide was provided. The full protein structure may prevent filament formation in these cases, and [URE3] induction by overproduction of the full-length protein may be initiated by proteolytic fragments. Our results imply that [URE3] is an infectious amyloidosis and suggest new approaches to the study of these diseases.

References and Notes

1. R. B. Wickner, *Science* **264**, 566 (1994).
2. J. Schoun and F. Lacroute, *C. R. Acad. Sci.* **269**, 1412 (1969); R. Drillien and F. Lacroute, *J. Bacteriol.* **109**, 203 (1972); T. G. Cooper, in *The Molecular Biology of the Yeast Saccharomyces*, J. N. Strathern, E. W. Jones, J. R. Broach, Eds. (Cold Spring Harbor Laboratory Press, Cold Spring Harbor, NY, 1982), vol. 2, p. 39; W. E. Courchesne and B. Magasanik, *J. Bacteriol.* **170**, 708 (1988); P. W. Coschigano and B. Magasanik, *Mol. Cell. Biol.* **11**, 822 (1991); B. Magasanik, in *The Molecular and Cellular Biology of the Yeast Saccharomyces*, E. W. Jones, J. R. Pringle, J. R. Broach, Eds. (Cold Spring Harbor Laboratory Press, Cold Spring Harbor, NY, 1992), vol. 2, p. 283.
3. I. Stansfield *et al.*, *EMBO J.* **14**, 4365 (1995); G. Zhouravleva *et al.*, *ibid.*, p. 4065.
4. F. Lacroute, *J. Bacteriol.* **106**, 519 (1971).
5. B. S. Cox, *Heredity* **20**, 505 (1965).
6. D. C. Masison and R. B. Wickner, *Science* **270**, 93 (1995).
7. Y. O. Chernoff, S. L. Lindquist, B.-I. Ono, S. G. Inge-Vechtomov, S. W. Liebman, *ibid.* **268**, 880 (1995).
8. S. V. Pausshkin, V. V. Kushnirov, V. N. Smirnov, M. D. Ter-Avanesyan, *EMBO J.* **15**, 3127 (1996).
9. _____, *Science* **277**, 381 (1997).

10. D. C. Masison, M.-L. Maddelein, R. B. Wickner, *Proc. Natl. Acad. Sci. U.S.A.* **94**, 12503 (1997).
11. T. Alper, W. A. Cramp, D. A. Haig, M. C. Clark, *Nature* **214**, 764 (1967); J. S. Griffith, *ibid.* **215**, 1043 (1967).
12. S. B. Prusiner, in *Fields Virology*, B. N. Fields, D. M. Knipe, P. M. Howley, Eds. (Raven, Philadelphia, 1996), vol. 2, pp. 2901-2950; B. Caughey and B. Chesebro, *Trends Cell Biol.* **7**, 56 (1997); C. Weissmann, *J. Biol. Chem.* **274**, 3 (1999).
13. G. G. Glenner, *N. Engl. J. Med.* **302**, 1333 (1980); R. Kisilevsky and P. E. Fraser, *Crit. Rev. Biochem. Mol. Biol.* **32**, 361 (1997).
14. K. L. Taylor and R. B. Wickner, unpublished data.
15. Ure2p¹⁻⁶⁵ and Ure2p¹⁴⁸⁻²¹³ were synthesized by G. Poy of the National Institute of Diabetes and Digestive and Kidney Diseases. Ure2p¹⁻⁶⁵ was purified by reverse-phase high-pressure liquid chromatography with a gradient of acetonitrile and trifluoroacetic acid. Electrospray mass spectrometry showed Ure2p¹⁻⁶⁵ and Ure2p¹⁴⁸⁻²¹³ had M⁺ values of 7103.3 and 7384.9, respectively. Fractions of Ure2p¹⁻⁶⁵ that contained ≥90% purified peptide were lyophilized. Ure2p¹⁴⁸⁻²¹³ was >70% pure.
16. Peptides Ure2p¹⁻⁶⁵, Ure2p¹⁴⁸⁻²¹³, and Aβ¹⁻⁴² were dissolved at 563, 542, and 554 μM, respectively, in 6 M guanidine hydrochloride (GuHCl), 50 mM tris-HCl, 0.2 M NaCl (pH 8). A protein mixture containing 54 μM thyroglobulin, 23 μM γ-globin, 83 μM ovalbumin, 107 μM myoglobin, 265 μM vitamin B₁₂, 106 μM ribonuclease A, 54 μM BSA, 23 μM aldolase (Bio-Rad and Pharmacia gel filtration standards) or 54 μM bovine serum albumin alone was prepared in 50 mM tris-HCl containing 0.2 M NaCl (pH 8.0). The aggregation reaction mixtures (126 μl) containing 13 μM Ure2p (17) or 0.16 volume of protein mixture or both in 50 mM tris-HCl (pH 8.0) containing 0.2 M NaCl were filter-sterilized and peptides were diluted into the protein solutions to a final concentration of 13 μM. Controls included 0.14 M guanidine and 13 μM Ure2p without the peptide. Reaction mixtures were gently rocked continuously at 8°C for 20 hours. The aggregated protein was collected by centrifugation for 1 min at 8500g and washed with buffer. Pellets were boiled for 5 min in 10 μl of SDS-polyacrylamide gel electrophoresis (SDS-PAGE) loading buffer and 30 μl of 8 M urea and then analyzed by SDS-PAGE.
17. Strain 3947 pKT18 (30) was grown in 100 liters of synthetic complete medium without leucine to OD₅₅₀ = 5.0 and the cells were stored at -80°C. Cell paste (180 g) was suspended in 1.5 volumes of lysis buffer [5 mM imidazole, 500 mM NaCl, 50 mM tris-HCl (pH 7.9) containing 1 mM phenylmethylsulfonyl fluoride (PMSF), aprotinin at 2 μg/ml, leupeptin at 2 μg/ml, and pepstatin at 2 μg/ml]. Cells were disrupted with a Bead-Beater (BioSpec Products) with 300 g of 0.5-mm glass beads twice for 4 min and then cooled with an ethanol-water ice bath. The lysate was centrifuged for 5 min at 10,000g and the supernatant was centrifuged for 20 min at 30,000g. The supernatant was applied at 2.5 ml/min to a 6-ml Ni-NTA superflow column (Qiagen). The column was washed with 10 volumes of lysis buffer and His₆-Ure2p was eluted with a 0 to 0.5 M imidazole gradient over 30 min at 1 ml/min. Fractions containing His₆-Ure2p according to SDS-PAGE and immunoblot analysis were pooled and concentrated. Concentrated protein was applied and eluted on a Superdex 200 HR 10/30 column (Pharmacia) in 50 mM tris-HCl (pH 8.0) containing 0.2 M NaCl.
18. B. Seilheimer *et al.*, *J. Struct. Biol.* **119**, 59 (1997); S. W. Snyder *et al.*, *Biophys. J.* **67**, 1216 (1994).
19. Data not shown.
20. In 750 μl, 5 μg of proteinase K was added to 50 μg of protein in 50 mM tris-HCl (pH 7.5) containing 0.15 M NaCl and was incubated at 37°C. At 0, 1, 2, 5, 10, and 15 min the reaction was quenched by the addition of 40 μl of SDS-PAGE loading buffer with 2 mM PMSF and 30 μl of 8 M urea to 120 μl of the reaction mixture. Samples were boiled and 25-μl aliquots were loaded onto 10 to 20% SDS-polyacrylamide gel. The gels were blotted onto polyvinylidene difluoride membranes and immunoblots were probed with an antibody specific for the NH₂-terminal region of Ure2p (7). Proteinase K digestion of mixed fibers for

REPORTS

electron microscopy was done for 15 min under similar conditions with 3.75-fold higher protease and protein concentrations.

21. G. C. Glenner, *Prog. Histochem. Cytochem.* **13**, 1 (1981).

22. Aggregated protein or peptide suspensions were mixed with 0.1 volume of 2% (w/v) CR (Sigma) and, after 1 hour at 20°C, were centrifuged at 8500g for 30 s. The aggregates were washed twice with 100 μ l of water. Aggregates were suspended in an equal volume of water and 10 μ l was placed on a glass slide and allowed to dry. Excess CR was removed by washing with 90% ethanol. Samples were viewed by polarization microscopy using a Zeiss Axialfold microscope equipped with optimally aligned cross-polarizers.

23. W. E. Klunk, J. W. Pettegrew, D. J. Abraham, *J. Histochem. Cytochem.* **37**, 1293 (1989).

24. H. K. Edskes, V. T. Gray, and R. B. Wickner, *Proc. Natl. Acad. Sci. U.S.A.*, in press.

25. C.-Y. King *et al.*, *ibid.* **94**, 6618 (1997).

26. J. R. Glover *et al.*, *Cell* **89**, 811 (1997).

27. M. M. Patino, J.-J. Liu, J. R. Glover, S. Lindquist, *Science* **273**, 622 (1996).

28. G. C. Glenner *et al.*, *ibid.* **174**, 712 (1971).

29. After the Ni-NTA step, Ure2p aggregates were formed on dialysis against <0.15 M NaCl in 50 mM tris-HCl (pH 7.5). However, these aggregates were amorphous and had no filament structure.

30. Plasmid construction: a His₆-URE2 fusion was constructed by polymerase chain reaction (PCR) with primers (5'-CGCGGATCCAAAAAATGCATCACCATC-ACCATCATGATGATGAATAACAACGGC-3') and (5'-G-GAACTGTCGACGAATCTGTGTTGGGGTAAC-3'). The purified PCR product was digested with Bam HI and Sal I and ligated to Bam HI- and Xho I-treated pH7 vector (24) (derived from pRS425 and containing LEU2 and the ADH1 promoter). This construct (pKT18) was checked by sequencing. Strain 3947

(*MAT α kar1 ure2 Δ ura2 Δ leu2 ade5 trp1 pep4::HIS3 GAL+*) carrying pKT18 (His₆-URE2 fusion) did not take up ureidosuccinate, showing that the URE2 fusion was functional. [URE3] could be cytoduced from strain 3310 [URE3-1] (*MAT α kar1 arg1* [URE3]) into strain 3947 containing pKT18 showing that the fusion protein could assume the prion form. These clones, made [ure-0] by growth to single colonies on minimal medium containing 5 mM GuHCl, were used for purification of Ure2p.

31. R. W. Williams, *J. Mol. Biol.* **166**, 581 (1983); in *Enzyme Structure*, C. H. W. Hirs and S. N. Timasheff, Eds. (Academic Press, New York, 1986), vol. 130, pp. 311-331.

32. We thank P. McPhie for help with spectroscopy, G. Poy for synthetic peptides, L. Pannell for mass spectrometry, and H. Edskes for plasmid pH7.

3 December 1998; accepted 25 January 1999

A Glial-Neuronal Signaling Pathway Revealed by Mutations in a Neurexin-Related Protein

Li-Lian Yuan* and Barry Ganetzky†

In the nervous system, glial cells greatly outnumber neurons but the full extent of their role in determining neural activity remains unknown. Here the axotactin (*axo*) gene of *Drosophila* was shown to encode a member of the neurexin protein superfamily secreted by glia and subsequently localized to axonal tracts. Null mutations of *axo* caused temperature-sensitive paralysis and a corresponding blockade of axonal conduction. Thus, the AXO protein appears to be a component of a glial-neuronal signaling mechanism that helps to determine the membrane electrical properties of target axons.

Glial cells influence neural activity indirectly by insulating neurons and regulating their microenvironment, but they also have direct effects on neuronal signaling and plasticity (1). The molecules responsible for mediating

communication between neurons and glia are largely unknown.

Neurexins are a family of neuronal cell surface proteins with proposed roles in cell adhesion and intercellular signaling (2).

Three distinct genes encoding neurexins have been identified in vertebrates. Neurexins, together with the closely related NCP protein family [defined by *Drosophila* and human neurexin IV, along with rat contactin-associated protein (Caspr, also known as paranodin)], constitute a protein superfamily (2). Studies indicate that members of the NCP family are involved in neuronal-glia interactions in both vertebrates and invertebrates. *Drosophila* neurexin IV mutants (*nrx IV*) disrupt septate junctions and impair the blood-brain barrier (3). Vertebrate Caspr may also mediate glial-dependent insulation of axons (4). The protein binding domains in the

Neuroscience Training Program and Laboratory of Genetics, 445 Henry Mall, University of Wisconsin-Madison, Madison, WI 53706 USA.

*Present address: Division of Neuroscience, Baylor College of Medicine, Houston, TX 77030, USA.

†To whom correspondence should be addressed. E-mail: ganetzky@facstaff.wisc.edu

Fig. 1. Molecular analysis of the *axo* locus. (A) Genomic structure of the *axo* locus. The exon-intron boundaries of *axo* were determined from genomic sequence analysis. Three genes (*axo*, gene *b*, and gene *c*) are localized in the vicinity of the P-element insertion site as determined by Northern blot and cDNA analysis. The *axo* gene contains at least 13 exons that span more than 45 kb of genomic DNA. The P element (vertical arrow) is inserted 23 bases upstream of the first exon of *axo*. The entire transcript of gene *b* is nested within the fifth intron of *axo*. The transcript of gene *c* is located upstream of *axo* on the other side of the P element. The direction of each transcript is indicated by horizontal arrows. The *axo*²⁸ allele is associated with a deletion of at least 10 kb at the 3' end of the *axo* locus. The location of the deletion is indicated by the horizontal line. One deletion breakpoint is localized between exons 11 and 12, as determined by genomic PCR. The location of the other breakpoint is not determined (indicated by a dashed line). The genomic structure of gene *c* is not completely mapped. (B) Northern blot analysis of *axo* and gene *b*. *axo* cDNA probes recognize a 7.5-kb band in the lane representing mRNA prepared from wild-type adult flies. This 7.5-kb band is undetectable in *axo*^{P12} mutants and is fully restored in two *axo*^{P12} revertants, *axo*^{P12-R1} (R1) and *axo*^{P12-R2} (R2). Complementary DNA probes from gene *b* recognize a 1.7-kb band. Neither this transcript nor the 4.2-kb transcript recognized by cDNA probes from gene *c* (not shown) is altered in the *axo*^{P12} mutant. (C) Diagram of the structural organization of *axo* as compared with that of members of the neurexin superfamily. The other proteins represented are *Drosophila* neurexin IV (NRX IV), rat Caspr/paranodin, and rat neurexin α (2-4). Gaps (dotted lines) are introduced into the sequences of the other proteins to maximize their alignment with the AXO sequence. The percent amino acid identity between the different domains in AXO and the corresponding domains in NRX IV or neurexin α is shown. The asterisk indicates that the two domains are less than 20% identical. The cysteine-rich Kunitz-like domain is present only in AXO. In addition, all the other proteins except AXO contain a transmembrane domain. DISC, discoidin domain.

